Plasmonic Smart Dust for Probing Local Chemical Reactions

ARTICLE *in* NANO LETTERS · MARCH 2013

Impact Factor: 13.59 · DOI: 10.1021/nl4005089 · Source: PubMed

8 AUTHORS, INCLUDING:

Andreas Tittl
École Polytechnique Fédérale de Lausanne
22 PUBLICATIONS **199** CITATIONS
SEE PROFILE

Zhong-Qun Tian
Xiamen University
356 PUBLICATIONS **10,171** CITATIONS
SEE PROFILE

Christian Kremers
Bergische Universität Wuppertal
28 PUBLICATIONS **276** CITATIONS
SEE PROFILE

Dmitry N. Chigrin
RWTH Aachen University
128 PUBLICATIONS **1,398** CITATIONS
SEE PROFILE

NANO LETTERS

Letter

pubs.acs.org/NanoLett

Plasmonic Smart Dust for Probing Local Chemical Reactions

Andreas Tittl,[†] Xinghui Yin,[†] Harald Giessen,[†] Xiang-Dong Tian,[‡] Zhong-Qun Tian,[‡] Christian Kremers,[§] Dmitry N. Chigrin,[§,⊥] and Na Liu*[,∥]

[†]4h Physics Institute and Research Center Scope, University of Stuttgart, D-70569 Stuttgart, Germany

[‡]State Key Laboratory for Physical Chemistry of Solid Surfaces and Department of Chemistry, College of Chemistry and Chemical Engineering, Xiamen University, Xiamen 361005, China

[§]Institute of High-Frequency and Communication Technology, Faculty of Electrical, Information and Media Engineering, University of Wuppertal, D-42119 Wuppertal, Germany

[∥]Max Planck Institute for Intelligent Systems, Heisenbergstrasse 3, D-70569 Stuttgart, Germany

Supporting Information

ABSTRACT: Locally probing chemical reactions or catalytic processes on surfaces under realistic reaction conditions has remained one of the main challenges in materials science and heterogeneous catalysis. Where conventional surface interrogation techniques usually require high-vacuum conditions or ensemble average measurements, plasmonic nanoparticles excel in extreme light focusing and can produce highly confined electromagnetic fields in subwavelength volumes without the need for complex near-field microscopes. Here, we demonstrate an all-optical probing technique based on plasmonic smart dust for monitoring local chemical reactions in real time. The silica shell-isolated gold nanoparticles that form the smart dust can work as strong light concentrators and optically report subtle environmental changes at their pinning sites on the probed surface during reaction processes. As a model system, we investigate the hydrogen dissociation and subsequent uptake trajectory in palladium with both "dust-on-film" and "film-on-dust" platforms. Using time-resolved single particle measurements, we demonstrate that our technique can in situ encode chemical reaction information as optical signals for a variety of surface morphologies. The presented technique offers a unique scheme for real-time, label-free, and high-resolution probing of local reaction kinetics in a plethora of important chemical reactions on surfaces, paving the way toward the development of inexpensive and high-output reaction sensors for real-world applications.

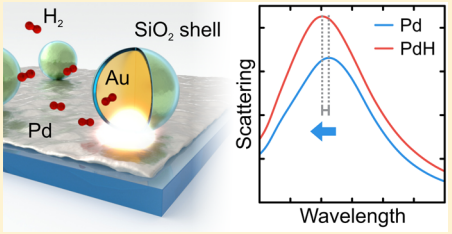

KEYWORDS: *Plasmonics, smart dust, local chemical reactions, palladium, hydrogen sensing*

The accelerating development of energy and chemical conversion technologies calls for a comprehensive understanding of physical and chemical processes on the nanoscale.[1] As size decreases, the importance of localized features such as shapes, facets, defects, and boundaries in nanostructures grows, giving rise to unpredictable changes in activity and behavior.[2] Probing and controlling local chemical reactions on the nanoscale is crucial and will enable significant progress in nanochemistry, especially in nanocatalysis where unanswered questions abound.[3−5] Conventional probing methods often rely on ultrahigh vacuum conditions.[6,7] Scanning tunneling microscopy, for example, offers a unique tool to gain insight into well-defined reaction systems but has difficulties to provide pervasive information at realistic reaction conditions. Surface-enhanced Raman spectroscopy is a powerful alternative to characterize the kinetics of chemical reactions.[8] However, the interpretation of Raman spectra can be time-consuming as trace contaminants may contribute additional peaks. Tip-enhanced Raman spectroscopy (TERS) allows for the investigation of arbitrary substrates[9,10] but suffers from weak Raman scattering signals.[11,12] Also, the fabrication of robust, reproducible, and highly enhancing tips is still challenging. Thus, there is a critical unmet need for sensitive, robust, and easy to implement techniques to probe local chemical reactions while they occur under diverse environmental conditions.

Plasmonic nanoparticles can concentrate light into a nanoscale volume, converting incident optical radiation into highly localized electromagnetic fields at a prescribed spot with subdiffraction-limit size.[13−20] In recent years, plasmonics has also branched out into other research fields, tackling intriguing problems in pharmacology, biology, and chemistry, among others.[21−27] For example, large plasmonic field-enhancements have been shown to significantly increase the efficiency of photocatalytic water splitting for hydrogen production, laying the groundwork for solar to chemical energy conversion.[28] Burning hydrogen produces no pollutants, making it an ideal candidate for clean energy storage and conversion in an economy increasingly based on green fuels. Consequently, safe chemical hydrogen storage requires the sensitive and reliable detection of hydrogen uptake in such materials.[29−36]

Received: February 8, 2013
Revised: March 1, 2013
Published: March 4, 2013

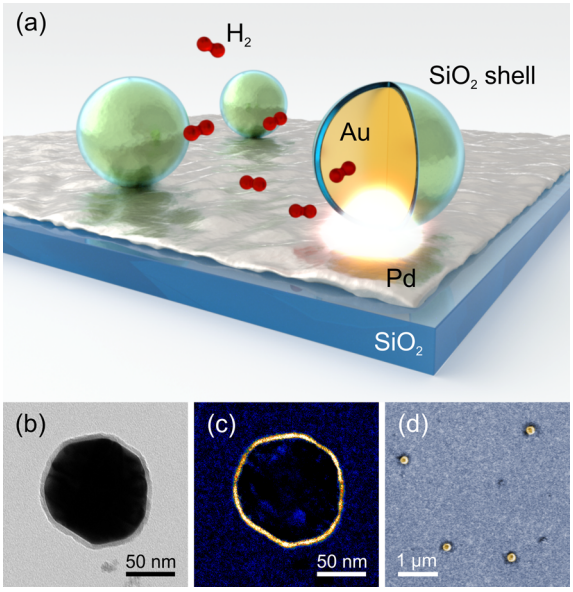

Figure 1. Plasmonic probing of local chemical reactions. (a) Sketch of the probing platform. Plasmonic smart dust (shell-isolated Au nanoparticles) are spread on a thin Pd film to locally probe diffusion of atomic hydrogen in Pd. (b) Exemplary TEM bright-field image of a smart dust nanoparticle deposited on a carbon membrane. (c) Energy-filtered TEM image using the Si L-edge of the same nanoparticle. The orange color indicates the presence of Si. The homogeneity of the ultrathin SiO_2 shell is excellent. (d) Exemplary SEM image of the smart dust deposited on a 15 nm thick Pd film via drop-coating. The particle separations are ideal for single-particle spectroscopy.

Here, we demonstrate all-optical probing of local chemical reactions along with hydrogen uptake in palladium (Pd) using single shell-isolated gold (Au) nanoparticles (Figure 1a). These nanoparticles, spread as plasmonic smart dust at reaction sites, can transduce local chemical reaction information into optical spectral changes in real time. The reactions under consideration involve the chemisorption of hydrogen molecules on the Pd surface, their near barrierless dissociation, and the diffusion of atomic hydrogen into Pd to form palladium hydride (PdH).[37,38] The Au core concentrates strong electromagnetic near-fields into a subwavelength volume adjacent to the Pd film, where the chemical reactions take place. Simultaneously, the Au core serves as a plasmonic probe to report the local reaction processes during hydrogen uptake through the dielectric changes of Pd at varying hydrogen concentrations. The scattering spectra of single plasmonic smart dust particles are recorded in situ by dark-field microscopy. Importantly, the ultrathin SiO_2 shell of the smart dust separates the Au core from direct contact with the probed agents. This constitutes a clear advantage of our platform over TERS-based methods that require complex tip-to-sample approaches, whereas our smart dust can simply be spread onto a catalytic or reactive surface. Our method also allows for simultaneous imaging of chemical processes at different reaction sites, combining indirect plasmonic sensing[29] and the highly uniform core−shell nanoprobes previously developed for SERS enhancement.[27] Furthermore, the smart dust particles can work as resonant antennas whose plasmon resonance can be tuned to the excitation wavelength of a probing laser.

The plasmonic smart dust used in this study consists of chemically grown SiO_2 shell (10 nm) isolated Au nanoparticles (150 nm). Synthesis details can be found in the Supporting Information. Figure 1b presents an exemplary transmission electron microscopy (TEM) image of a smart dust nanoparticle. The energy-filtered TEM image using the Si L-edge of the same particle is shown in Figure 1c in which the Au core and the SiO_2 shell can be nicely distinguished. The key virtue of our plasmonic smart dust is its uniform and ultrathin SiO_2 shell, which allows the Au core to generate strong electromagnetic near-fields and simultaneously protects it from the chemical environment. To demonstrate the versatility of our approach for diverse surface morphologies, we investigate two representative probing platforms: "dust-on-film", where the plasmonic smart dust is dispersed on a thin Pd film, and "film-on-dust", where the smart dust is covered with a highly curved Pd film. In both cases, careful dilution and drop-coating of the smart dust yield samples with interparticle distances suitable for single-particle spectroscopy (Figure 1d).

We first investigate the dust-on-film platform as shown in the inset of Figure 2a. Here, the smart dust nanoparticles are dispersed on a thin Pd film, which resides on a quartz substrate. After placing the sample in a stainless-steel reaction chamber, the concentration of hydrogen during the reactions is controlled by tuning the ratio of high-purity hydrogen and nitrogen gas through mass-flow controllers. The hydrogen uptake processes are probed in situ by recording the scattering spectra of single smart dust particles. Experimental details are described in the Supporting Information. Figure 2a shows the complete time-resolved optical response of a single smart dust particle on a 15 nm Pd film at different hydrogen concentrations. Upon introducing hydrogen into the reaction chamber at concentrations as low as 0.5%, the resonance of the smart dust particle at roughly 600 nm shows an immediate response both in intensity and wavelength position, indicating the onset of hydrogen molecule dissociation and subsequent atomic hydrogen diffusion into the Pd. More specifically, the plasmonic resonance shifts to the blue and its intensity increases. Hydrogen uptake in Pd leads to a phase transition, turning it into more semiconductor-like than metal-like, which is manifested in its dielectric function change.[37,39] These changes are closely correlated with the amount of hydrogen stored in the Pd. Because of the strong electromagnetic near-fields associated with the plasmon excitation, the smart dust particle can capture this information arising from the chemical reactions at its specific location and converts it into optical spectral changes. As a result of the evanescent nature of particle plasmons, the smart dust particle works as a point probe that only conveys the hydrogen uptake information in a confined subwavelength sensing volume at its location. The information beyond this sensing volume is fully discarded, making it an ideal local reaction reporter.

To test the ability of our plasmonic smart dust for resolving different hydrogen contents in Pd, the sample is repeatedly exposed to hydrogen concentrations ranging from 0.5 to 3%. As shown in Figure 2a, different hydrogen concentrations can be clearly identified as intensity changes of the plasmonic resonance with response times on the order of seconds. The observed fast reaction kinetics compared to bulk palladium systems are due to the shorter diffusion lengths associated with Pd thin films and nanomaterials.[32] In general, higher hydrogen concentrations lead to increased resonance intensity and spectral blueshift of the resonance position.

To resolve the small spectral shifts associated with low hydrogen concentrations, we employ a centroid analysis method.[40] In contrast to simply tracking the scattering spectral

dx.doi.org/10.1021/nl4005089 | Nano Lett. 2013, 13, 1816−1821

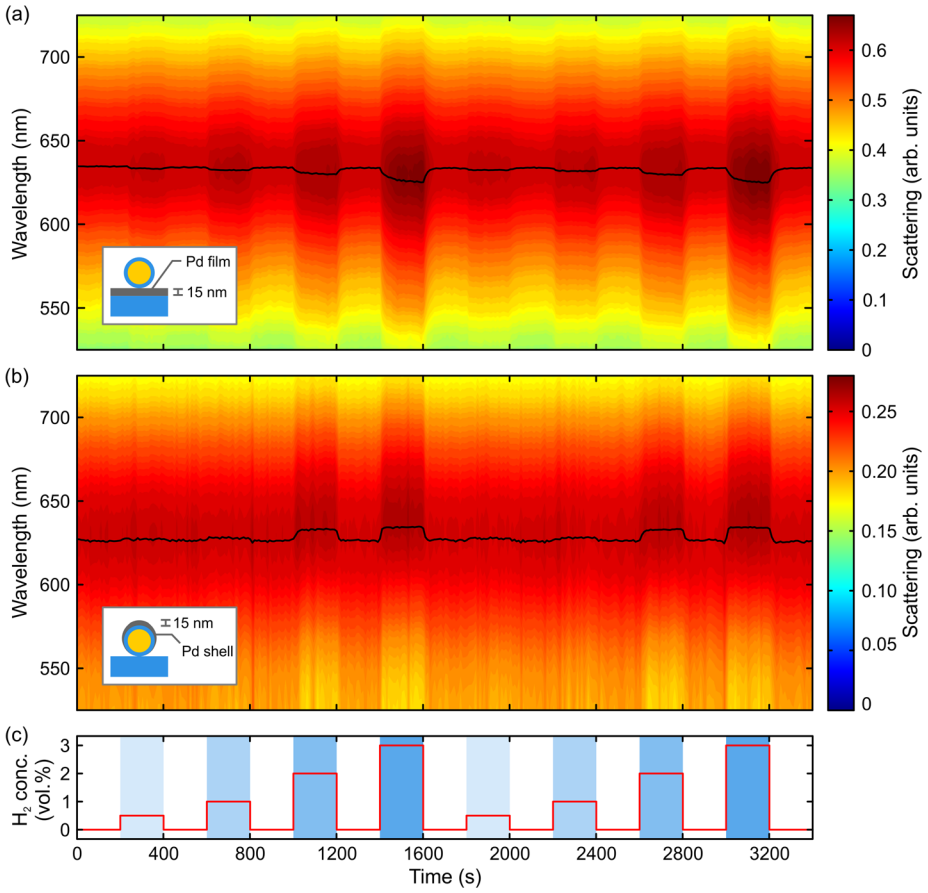

Figure 2. Optical trajectories of local hydrogen uptake and release. Color-coded spectral scattering intensity over time. (a) Dust-on-film, single smart dust particle on a 15 nm Pd film. (b) Film-on-dust, single smart dust particle covered by a 15 nm Pd film. In both cases, the black lines denote the centroid wavelengths and serve as guides to the eye. The plasmonic smart dust detects the local chemical reactions and converts the information into optical signal changes, which are manifested in resonance intensity and resonance position with a response time on the order of seconds. The single particle measurements are carried out using dark-field microscopy in real time. (c) Concentration of hydrogen in nitrogen carrier gas during the reactions.

maximum, the centroid method computes the "center of mass" of the scattering spectrum, providing a highly reliable way to determine the resonance wavelength position (see Supporting Information). In addition, a bootstrapping approach[41,42] is used to estimate the statistical error (standard deviation) of the retrieved centroid wavelength position.

To demonstrate the spatially confined nature of our plasmonic probes, we alter the local environment of the plasmonic smart dust by using a thinner Pd film (10 nm). We compare the time-resolved centroid wavelength position changes under the same reaction conditions for samples with 10 and 15 nm Pd films, respectively (Figure 3a,b). In both cases, clear shifts of the resonance position are observed upon hydrogen uptake and release. The 15 nm Pd sample displays a much more pronounced optical response compared to the 10 nm Pd sample at identical hydrogen concentrations. More specifically, the former exhibits a pronounced blue-shift as large as 8 nm at 3%, whereas the latter only leads to half of this blueshift value. A Pd film thickness change of 5 nm already suffices to induce a notable influence on the hydrogen storage behavior. In turn, this elucidates that our plasmonic smart dust can optically resolve the difference of hydrogen uptake processes arising from extremely small environmental changes at its probing site. This is of great importance for studies of heterogeneous catalysis, where local structural characteristics such as size, shape, geometry, and surface morphology of catalysts are crucial. For gaining a broader view, the plasmonic smart dust may be used to produce a local reaction map by pinning multiple nanoparticles at reaction sites of interest and optically monitoring spatially distinct local chemical reactions simultaneously.

To further demonstrate the ability of our plasmonic smart dust to probe local chemical reactions for more complex surface morphologies, we investigate the second sensor platform: film-on-dust (see the inset of Figure 2b). The plasmonic smart dust is dispersed on a quartz substrate and a Pd film (15 nm) is evaporated on the nanoparticles through titled angle evaporation, forming a highly curved Pd surface on the particles. The sample is then placed in the reaction chamber. The experimental procedures are the same as those in Figure 2a, and results are plotted in Figures 2b and 3c for the same smart dust particle. All concentration steps are again clearly identified through the changes of the optical response. The resonance intensity does not change as dramatically as that in the dust-on-film configuration. Still, the resonance exhibits a pronounced 8 nm red-shift at a hydrogen concentration of 3%. Strikingly, the direction of the spectral shift is reversed with respect to the dust-on-film case in Figure 2a. Our plasmonic smart dust can therefore sensitively distinguish subtle changes at its probing site, yielding large associated optical changes. This shows that

dx.doi.org/10.1021/nl4005089 | Nano Lett. 2013, 13, 1816−1821

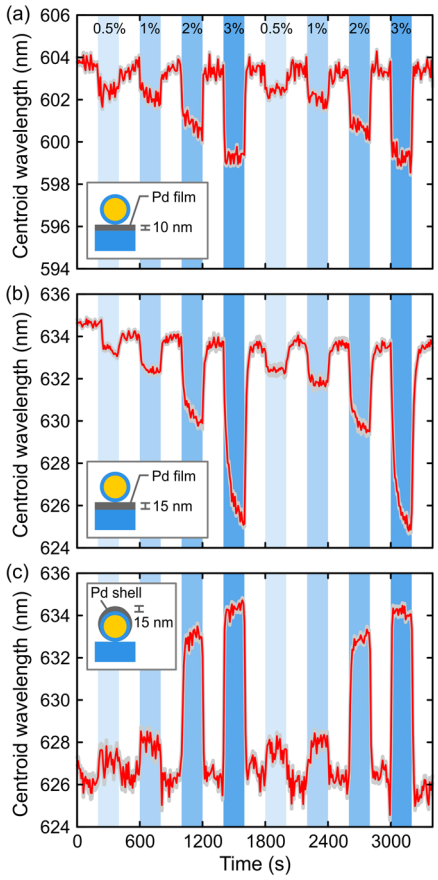

Figure 3. Experimental time-resolved centroid wavelengths in response to hydrogen uptake and release. (a) Dust-on-film, single smart dust particle on a 10 nm Pd film. (b) Dust-on-film, single smart dust particle on a 15 nm Pd film (same particle as in Figure 2a). The minute 5 nm film thickness change can easily be resolved optically under the same reaction conditions. (c) Film-on-dust, single smart dust particle covered by a 15 nm Pd film (same particle as in Figure 2b). The spectral response shifts completely to the opposite direction compared to that in the dust-on-film platform. This underlines the suitability of our technique for studying local reactions on various surface morphologies. Gray areas behind the red curves denote the errors of the centroid analysis, estimated using a bootstrapping method. The statistical error (standard deviation) of the calculated centroid wavelengths is below σ = 0.13 nm in all cases.

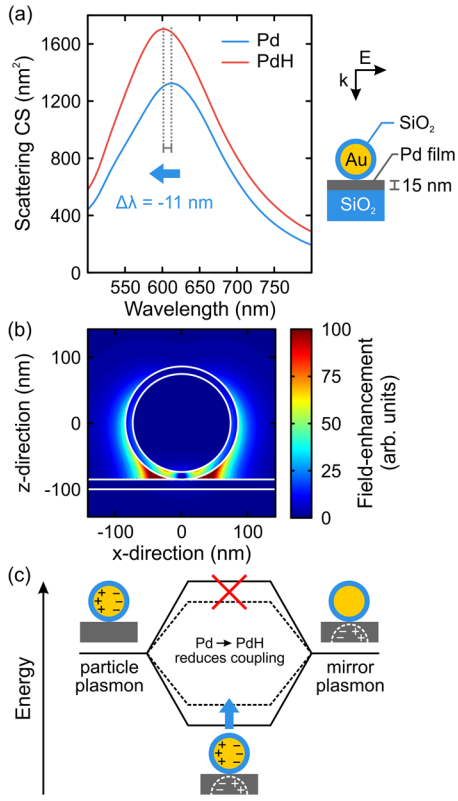

Figure 4. Numerical simulations for the dust-on-film platform. (a) Simulated scattering spectra for a single smart dust particle on an infinitely extended 15 nm Pd film before and after hydrogen uptake. A fully hydrided state PdH is used in the calculation to establish the maximum spectral shift in the reaction. A maximum blueshift of $\Delta\lambda$ = 11 nm together with a resonance intensity increase is predicted. (b) Electric near-field distribution at resonance. The intense near-fields are strongly localized at the touching point between the smart dust and the Pd film. (c) Hybridization model for interpreting the observed spectral blueshift. The localized plasmon of the Au nanoparticle hybridizes with the induced mirror plasmon in the Pd film, leading to the observed bonding mode. The higher energy antibonding mode is not allowed in this configuration. When changing from Pd to PdH, the properties of the film become less metallic. This leads to weaker plasmonic coupling and therefore a reduced energy splitting, resulting in a resonance blueshift.

our method can easily be adapted for a multitude of different surface morphologies and associated local chemical reactions. In addition, the low statistical error of the centroid wavelength position (standard deviation σ = 0.13 nm) together with a spectral shift of 1.5 nm at 0.5% hydrogen holds great promise for detecting low amounts of hydrogen in the part per million range.

To theoretically support our experimental observations, the scattering spectra of a plasmonic smart dust particle upon hydrogen uptake are calculated for the dust-on-film and film-on-dust platforms, respectively. The calculations were performed using a commercial implementation of the method of moments (MoM) based on the surface equivalence principle (FEKO 6.2). More details on the numerical simulations can be found in the Supporting Information. The calculated results for the dust-on-film configuration are shown in Figure 4a. In the case of a 15 nm Pd film, a clear spectral blue-shift of $\Delta\lambda$ = 11 nm together with an increase of the resonance intensity is predicted when changing the dielectric function of the film from pure Pd to fully hydrided Pd, that is, PdH.[39] In the experiment, the blueshift is around 8 nm at a hydrogen concentration of 3%, which is still below the fully hydrided state. Thus, the numerical calculations neatly confirm the trend of the spectral changes in response to hydrogen uptake in the experiment.

The highly localized nature of our plasmonic nanoprobe becomes evident from the simulated electric near-field distribution at resonance (Figure 4b). Intense near-fields are strongly concentrated around the touching point of the smart dust particle with the Pd film, allowing for the interrogation of local reactions with high spatial resolution. When linearly polarized light impinges on a smart dust nanoparticle, it excites an oscillating particle plasmon in the Au core. This charge distribution induces the oscillation of a mirror plasmon in the underlying Pd film. The particle and mirror plasmons mix and hybridize, resulting in a lower-energy bonding mode and a higher-energy antibonding mode (Figure 4c). The latter cannot be observed due to the parity of the mirrored charge

dx.doi.org/10.1021/nl4005089 | Nano Lett. 2013, 13, 1816–1821

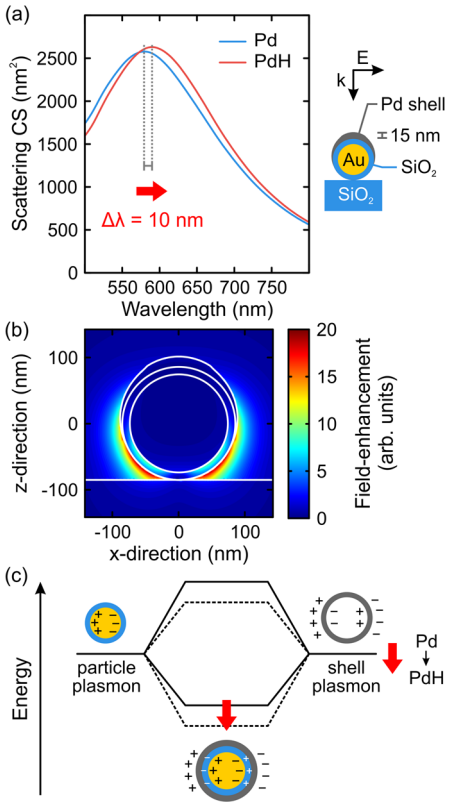

Figure 5. Numerical simulations for the film-on-dust platform. (a) Simulated scattering spectra for a single smart dust particle coated with a 15 nm Pd film. When changing the dielectric function of the shell from Pd to PdH, a redshift of $\Delta\lambda$ = 10 nm is predicted. The resonance intensity increase is not as large as that in Figure 4a. (b) Electric near-field distribution at resonance. The electric near-fields are more localized at the side surfaces of the smart dust, indicating resonant coupling of the particle plasmons in the Au and Pd parts of the structure. (c) Hybridization model for interpreting the observed spectral redshift. For clarity, a continuous Pd shell is utilized. The particle plasmon in the Au core hybridizes with the particle plasmon in the Pd shell, resulting in a lower-energy bonding mode and a higher-energy antibonding mode. When changing from Pd to PdH, the Pd shell plasmon shifts to a lower energy level, leading to a corresponding redshift of the bonding mode.

distribution.[43] When transitioning from Pd to PdH upon hydrogen uptake, the real part of the Pd film's dielectric function becomes less negative,[39] giving rise to a less metallic character of the film and thus weaker coupling between the particle and mirror plasmons. This leads to reduced plasmonic mode-splitting and the bonding mode shifts to a higher energy or, when considering wavelengths, to the blue. The reduction in metallic character during the Pd/PdH transition also explains the increase in the scattering amplitude due to increased light transmission through the film.

The numerical results for the film-on-dust platform are shown in Figure 5a. We again compare the scattering spectra for the Pd and PdH cases. In contrast to the dust-on-film platform, a resonance redshift of $\Delta\lambda$ = 10 nm upon hydrogen uptake is predicted and the resonance intensity increases only slightly due to the lack of a fully closed Pd film. All these spectral characteristics are in excellent agreement with the observations in our experiment.

Taking a further step, the electric near-field distribution at resonance is again calculated for this configuration (Figure 5b). Unlike the dust-on-film platform where a clear focusing of the near-fields at the base of the nanoparticle is observed, the intense fields are localized more at the side surfaces of the smart dust particle, indicating strong interaction between the gold core and the curved Pd shell. For simplicity, we utilize a continuous Pd shell around the dust particle in our hybridization model (Figure 5c). Here, the particle plasmon of the smart dust particle hybridizes with the particle plasmon excited in the Pd shell, leading to a lower-energy bonding and a higher-energy antibonding mode. Because of the large intrinsic damping in gold at short wavelengths, the antibonding mode is not clearly observable in the wavelength range of interest. When changing the dielectric function of the shell from Pd to PdH, the shell plasmon shifts to a lower energy, leading to a redshift of the bonding mode, which agrees well with the spectral shift trend in the experiment.

In conclusion, our versatile, all-optical technique offers a unique way to probe local chemical behavior and catalytic processes at individual reaction sites. The noninvasive nano-optical measurements circumvent the need and high expense of specialized equipment associated with conventional surface science characterization techniques. Our single-particle platform enables simultaneous probing of chemical reactions at various surface morphologies and local reaction environments under identical reaction conditions. By combining two-dimensional imaging and spectroscopic techniques, synchronized mapping and chemical sensing on a subdiffraction-limit scale could be achieved.[44,45] Our method can be extended to investigate a plethora of chemical reactions on surfaces, ranging from the reduction and oxidation steps in fuel cells[46,47] to catalytic water splitting.[48]

■ ASSOCIATED CONTENT

Supporting Information

Description of methods, derivation of the shell thickness in the film-on-dust case, and TEM image of several smart dust particles. This material is available free of charge via the Internet at http://pubs.acs.org.

■ AUTHOR INFORMATION

Corresponding Author

*E-mail: laura.liu@is.mpg.de.

Present Address

[⊥](D.N.C.) I. Physikalisches Institut, RWTH Aachen, D-52056 Aachen, Germany.

Author Contributions

N.L. and H.G. conceived the experiments. A.T. performed the experiments and analyzed the data. X.Y., C.K., and D.N.C. carried out the calculations. Z.T. and X.T. synthesized the nanoparticles. A.T., H.G., and N.L. wrote the manuscript. All authors contributed to revise the manuscript.

Notes

The authors declare no competing financial interests.

■ ACKNOWLEDGMENTS

The TEM measurements were performed by K. Hahn at Max Planck Institute for Intelligent Systems, Stuttgart, Germany. We acknowledge J. Zhao for help with the tilted evaporation. We are grateful to A. Muramatsu, N. Strohfeldt, and M. Hentschel for key advice and discussions. A.T., X.Y., and H.G. were financially supported by the DFG (SPP1391, FOR730, and GI 269/11-1), the BMBF (13N9049 and 13N10146), the Baden-

Württemberg Stiftung (Kompetenznetz Funktionelle Nanostrukturen), and the MWK Baden-Württemberg. N.L. was supported by the Sofia Kovalevskaja Award of the Alexander von Humboldt Foundation.

REFERENCES

(1) Linic, S.; Christopher, P.; Ingram, D. B. *Nat. Mater.* **2011**, *10*, 911−921.
(2) Watanabe, K.; Menzel, D.; Nilius, N.; Freund, H.-J. *Chem. Rev.* **2006**, *106*, 4301−4320.
(3) Fox, M. A.; Dulay, M. T. *Chem. Rev.* **1993**, *93*, 341−357.
(4) Ertl, G.; Freund, H.-J. *Phys. Today* **1999**, *52*, 32−38.
(5) Novo, C.; Funston, A. M.; Mulvaney, P. *Nat. Nanotechnol.* **2008**, *3*, 598−602.
(6) Mitsui, T.; Rose, M. K.; Fomin, E.; Ogletree, D. F.; Salmeron, M. *Nature* **2003**, *422*, 705−707.
(7) van Schrojenstein Lantman, E. M.; Deckert-Gaudig, T.; Mank, A. J. G.; Deckert, V.; Weckhuysen, B. M. *Nat. Nanotechnol.* **2012**, *7*, 583−586.
(8) Kim, H.; Kosuda, K. M.; Van Duyne, R. P.; Stair, P. C. *Chem. Soc. Rev.* **2010**, *39*, 4820−4844.
(9) Jiang, N.; Foley, E. T.; Klingsporn, J. M.; Sonntag, M. D.; Valley, N. A.; Dieringer, J. A.; Seideman, T.; Schatz, G. C.; Hersam, M. C.; Van Duyne, R. P. *Nano Lett.* **2012**, *12*, 5061−5067.
(10) Sonntag, M. D.; Klingsporn, J. M.; Garibay, L. K.; Roberts, J. M.; Dieringer, J. A.; Seideman, T.; Scheidt, K. A.; Jensen, L.; Schatz, G. C.; Van Duyne, R. P. *J. Phys. Chem. C* **2012**, *116*, 478−483.
(11) Pettinger, B.; Ren, B.; Picardi, G.; Schuster, R.; Ertl, G. *Phys. Rev. Lett.* **2004**, *92*, 96101.
(12) Wu, D.-Y.; Li, J. F.; Ren, B.; Tian, Z. Q. *Chem. Soc. Rev.* **2008**, *37*, 1025−1041.
(13) Halas, N. J.; Lal, S.; Chang, W.-S.; Link, S.; Nordlander, P. *Chem. Rev.* **2011**, *111*, 3913−3961.
(14) Lal, S.; Link, S.; Halas, N. J. *Nat. Photonics* **2007**, *1*, 641−648.
(15) Novotny, L.; van Hulst, N. *Nat. Photonics* **2011**, *5*, 83−90.
(16) Becker, J.; Zins, I.; Jakab, A.; Khalavka, Y.; Schubert, O.; Sönnichsen, C. *Nano Lett.* **2008**, *8*, 1719−1723.
(17) Maier, S. A. *Plasmonics: Fundamentals and Applications*; Springer: New York, 2007.
(18) Zheludev, N. I.; Kivshar, Y. S. *Nat. Mater.* **2012**, *11*, 917−924.
(19) Ciracì, C.; Hill, R. T.; Mock, J. J.; Urzhumov, Y.; Fernández-Domínguez, A. I.; Maier, S. A.; Pendry, J. B.; Chilkoti, A.; Smith, D. R. *Science* **2012**, *337*, 1072−1074.
(20) Hill, R. T.; Mock, J. J.; Hucknall, A.; Wolter, S. D.; Jokerst, N. M.; Smith, D. R.; Chilkoti, A. *ACS Nano* **2012**, *6*, 9237−9246.
(21) Wu, H.-J.; Henzie, J.; Lin, W.-C.; Rhodes, C.; Li, Z.; Sartorel, E.; Thorner, J.; Yang, P.; Groves, J. T. Membrane-protein binding measured with solution-phase plasmonic nanocube sensors. *Nat. Methods* **2012**, *9*, 1189−1191.
(22) de la Rica, R.; Stevens, M. M. Plasmonic ELISA for the ultrasensitive detection of disease biomarkers with the naked eye. *Nat. Nanotechnol.* **2012**, *7*, 821−824.
(23) Choi, Y.; Park, Y.; Kang, T.; Lee, L. P. *Nat. Nanotechnol.* **2009**, *4*, 742−746.
(24) Anker, J. N.; Hall, W. P.; Lyandres, O.; Shah, N. C.; Zhao, J.; Van Duyne, R. P. *Nat. Mater.* **2008**, *7*, 442−453.
(25) Wu, C.; Khanikaev, A. B.; Adato, R.; Arju, N.; Yanik, A. A.; Altug, H.; Shvets, G. *Nat. Mater.* **2012**, *11*, 69−75.
(26) Yanik, A. A.; Huang, M.; Kamohara, O.; Artar, A.; Geisbert, T. W.; Connor, J. H.; Altug, H. *Nano Lett.* **2010**, *10*, 4962−4969.
(27) Li, J. F.; Huang, Y. F.; Ding, Y.; Yang, Z. L.; Li, S. B.; Zhou, X. S.; Fan, F. R.; Zhang, W.; Zhou, Z. Y.; Wu, De Yin; Ren, Bin; Wang, Z. L.; Tian, Z. Q. *Nature* **2010**, *464*, 392−395.
(28) Liu, Z.; Hou, W.; Pavaskar, P.; Aykol, M.; Cronin, S. B. *Nano Lett.* **2011**, *11*, 1111−1116.
(29) Liu, N.; Tang, M. L.; Hentschel, M.; Giessen, H.; Alivisatos, A. P. *Nat. Mater.* **2011**, *10*, 631−636.
(30) Tittl, A.; Mai, P.; Taubert, R.; Dregely, D.; Liu, N.; Giessen, H. *Nano Lett.* **2011**, *11*, 4366−4369.
(31) Langhammer, C.; Zorić, I.; Kasemo, B.; Clemens, B. M. *Nano Lett.* **2007**, *7*, 3122−3127.
(32) Langhammer, C.; Zhdanov, V. P.; Zorić, I.; Kasemo, B. *Phys. Rev. Lett.* **2010**, *104*, 135502.
(33) Seo, D.; Park, G.; Song, H. *J. Am. Chem. Soc.* **2012**, *134*, 1221−1227.
(34) Tang, M. L.; Liu, N.; Dionne, J. A.; Alivisatos, A. P. *J. Am. Chem. Soc.* **2011**, *133*, 13220−13223.
(35) Buso, D.; Post, M.; Cantalini, C.; Mulvaney, P.; Martucci, 2. *Adv. Funct. Mater.* **2008**, *18*, 3843−3849.
(36) Poyli, M. A.; Silkin, V. M.; Chernov, I. P.; Echenique, P. M.; Muiño, R. D.; Aizpurua, J. *J. Phys. Chem. Lett.* **2012**, *3*, 2556−2561.
(37) Flanagan, T. B.; Oates, W. A. *Annu. Rev. Mater. Sci.* **1991**, *21*, 269−304.
(38) Gross, A. *Appl. Phys. A* **1998**, *67*, 627−635.
(39) Vargas, W. E.; Rojas, I.; Azofeifa, D. E.; Clark, N. *Thin Solid Films* **2006**, *496*, 189−196.
(40) Dahlin, A. B.; Tegenfeldt, J. O.; Höök, F. *Anal. Chem.* **2006**, *78*, 4416−4423.
(41) Efron, B. *Ann. Stat.* **1979**, *7*, 1−26.
(42) Efron, B. *Biometrika* **1981**, *68*, 589−599.
(43) Liu, N.; Guo, H.; Fu, L.; Kaiser, S.; Schweizer, H.; Giessen, H. *Adv. Mater.* **2007**, *19*, 3628−3632.
(44) Shan, X.; Díez-Pérez, I.; Wang, L.; Wiktor, P.; Gu, Y.; Zhang, L.; Wang, W.; Lu, J.; Wang, S.; Gong, Q.; Li, J.; Tao, N. *Nat. Nanotechnol.* **2012**, *7*, 668−672.
(45) Barth, M.; Schietinger, S.; Fischer, S.; Becker, J.; Nüsse, N.; Aichele, T.; Löchel, B.; Sönnichsen, C.; Benson, O. *Nano Lett.* **2010**, *10*, 891−895.
(46) Zhang, J.; Vukmirovic, M. B.; Xu, Y.; Mavrikakis, M.; Adzic, R. R. *Angew. Chem., Int. Ed.* **2005**, *44*, 2132−2135.
(47) Park, S.; Vohs, J.; Gorte, R. *Nature* **2000**, *404*, 265−267.
(48) Zou, Z.; Ye, J.; Sayama, K.; Arakawa, H. *Nature* **2001**, *414*, 625−627.

NOTE ADDED AFTER ASAP PUBLICATION

This article was published ASAP on March 7, 2013. The caption to Figure 1, one paragraph in the text, and the Supporting Information have been modified. The corrected version was published on March 22, 2013.